

# Light hadron spectra and wave functions in quenched QCD with overlap quarks on a large lattice<sup>\*†</sup>

F. Berruto<sup>a</sup>, N. Garron<sup>b</sup>, C. Hoelbling<sup>b‡</sup>, J. Howard<sup>c</sup>, L. Lellouch<sup>b</sup>, S. Necco<sup>b</sup>, C. Rebbi<sup>c</sup>, and N. Shoresh<sup>c§</sup>

<sup>a</sup>Department of Physics, Brookhaven National Laboratory, Upton NY 11973, USA

<sup>b</sup>Centre de Physique Théorique<sup>1</sup>, Case 907, CNRS Luminy, F-13288 Marseille Cedex 9, France

<sup>c</sup>Department of Physics, Boston University, 590 Commonwealth Avenue, Boston MA 02215, USA

A simulation of quenched QCD with the overlap Dirac operator has been completed using 100 Wilson gauge configurations at  $\beta = 6$  on an  $18^3 \times 64$  lattice. We present results for meson and baryon masses, meson final state “wave functions” and other observables.

## 1. Simulation Details

We have studied quenched QCD on an  $18^3 \times 64$  lattice, with the Wilson gauge action at  $\beta = 6$  and with Neuberger’s overlap Dirac operator for lattice fermions. We used a sample of 100 gauge configurations separated by 10,000 upgrades of a 6-hit Metropolis algorithm (acceptance  $\simeq 0.5$ ). A previous preliminary analysis [1] used the first 60 quark propagators that were produced; results presented here include all 100 quark propagators. We refer to [1] and the references therein for more background information and details of the overlap operator used. New results include the vector meson spectrum, the use of extended sink operators in constructing meson correlation functions, and observation of quenched chiral logs. Results for kaon weak matrix elements are presented in a separate contribution [2].

From Wilson loops, we obtained  $r_0/a = 5.36 \pm$

0.11 ( $a^{-1} = 2.11 \pm 0.04$  GeV) for the Sommer scale defined by  $r_0^2 F(r_0) = 1.65$ ,  $r_0 = 0.5$  fm.

We calculated overlap quark propagators for a single point source, for all 12 color-spin combinations and quark masses  $am_q = 0.03, 0.04, 0.06, 0.08, 0.1, 0.25, 0.5, 0.75$ , using a multi-mass solver.

The Zolotarev approximation with 12 poles was used for the first 55 configurations. For the remaining 45 configurations, the Chebyshev approximation (degree 100  $\sim$  500) was used, after Ritz projection of the lowest 12 eigenvectors of  $H^2$ , as it was found to provide about 20% better performance. The convergence criterion used was  $|D^\dagger D\psi - \chi|^2 < 10^{-7}$ .

The computations were performed with shared memory F90 code, optimized and run on 16 and 32 processor IBM-p690 nodes at BU and NCSA.

## 2. Meson Results

We begin with a verification of the axial Ward identity (AWI) prediction for the ratio

$$\rho(t) = G_{\nabla_0 A_0 P}(t)/G_{PP}(t) \quad (1)$$

as presented in Fig. 1. The fit to  $a\rho = A + a(m_{q1} + m_{q2})/Z_A + C[a(m_{q1} + m_{q2})]^2$  gives  $A = (3.09 \pm 9.57) \times 10^{-6}$ ,  $Z_A = 1.5570 \pm 0.0004$ , and  $C = (-5.12 \pm 0.61) \times 10^{-3}$ , as shown in Fig. 2.

<sup>\*</sup>Work supported in part by US DOE grants DE-FG02-91ER40676 and DE-AC02-98CH10866, EU contracts HPRN-CT-2000-00145 and HPRN-CT-2002-00311, and grant HPMF-CT-2001-01468. We thank Boston University and NCSA for use of their supercomputer facilities.  
<sup>†</sup>Combined presentations by J. Howard, L. Lellouch and C. Rebbi at *Lattice 2004*, FNAL, USA.

<sup>‡</sup>Present address: Department of Physics, Bergische Universität Wuppertal, Gausstr. 20, D-42119, Germany

<sup>§</sup>Now at Harvard University.

<sup>1</sup>UMR 6207 du CNRS et des universités d’Aix-Marseille I, II et du Sud Toulon-Var, affiliée à la FRUMAM.

2

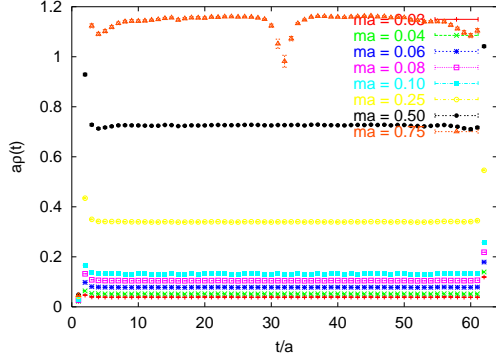


Figure 1. AWI ratio as a function of time for all degenerate quark mass combinations.

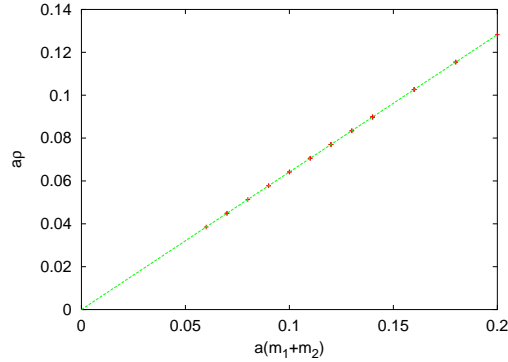


Figure 2. Axial Ward identity, continued.

## 2.1. Meson Spectrum

Pseudoscalar density 2-point functions were formed from quark propagators and then fit to the usual cosh form to calculate the ground state mass. An example correlator is shown in Fig. 3, for input quark masses  $am_{q1} = 0.08$  and  $am_{q2} = 0.10$ .

Effective mass plots are often used to determine the fitting window  $\{t_{min}, t_{max}\}$  for the correlation function. In some cases (e.g. for vector mesons), determining the best window can be difficult. Therefore, we used a method that scanned the possible windows, and then chose the smallest value of  $t_{min}$  (consistent with the errors) allowed before the clear effect of higher states caused the mass prediction to rise. Use of a cosh fit allowed

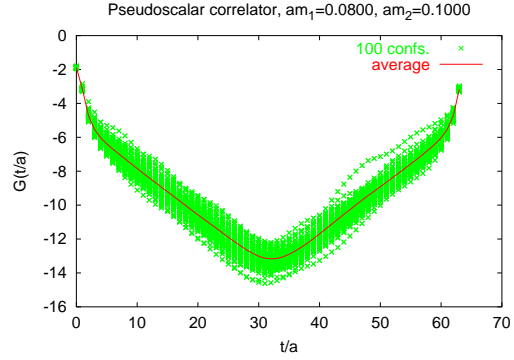


Figure 3. Time dependence of a pseudoscalar correlator. Its value on each gauge configuration as well as its average value are shown.

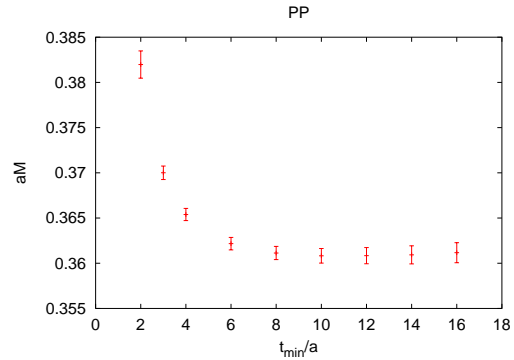


Figure 4. Scanning the window for optimum  $t_{min}$ .

$t_{max}$  to be fixed at 32. An example of such a scan is shown in Fig. 4. The pseudoscalar spectrum for all possible input quark mass combinations is shown in Fig. 5. Using a larger lattice than [3] allowed for observation of vector meson states, as shown in Fig. 6.

## 2.2. Extended sink operators

Since mesons are not point particles, an increased signal can be obtained by using extended (or smeared) operators at the source and sink [4]. Matrix element calculations required point sources and generating an additional set of propagators with extended sources would have been computationally too costly. Thus we limited

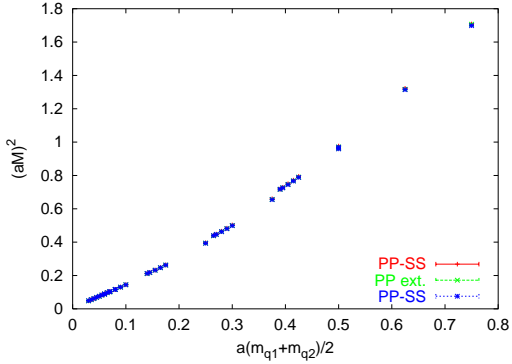


Figure 5. Pseudoscalar spectrum.

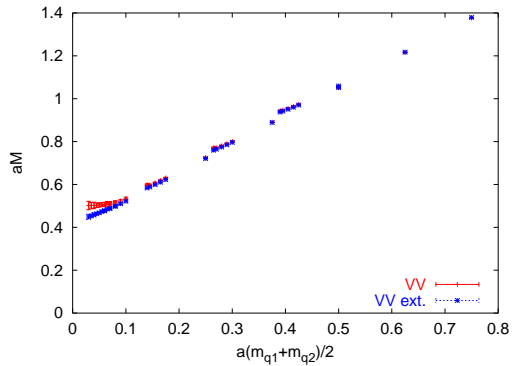


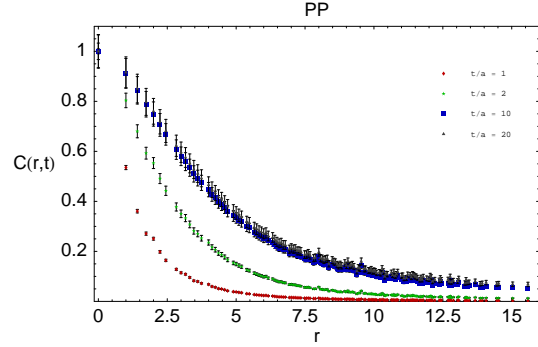
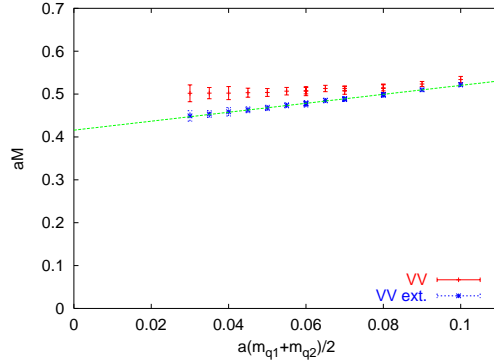
Figure 6. Vector meson spectrum for point and extended sinks.

our analysis to extended sinks.

The use of extended sinks allowed for a larger fitting window and improved the prediction for mesonic observables. The extended sink correlation function is

$$G_f(t) = \langle \sum_{\mathbf{x}, \mathbf{y}} \bar{\psi}(\mathbf{x}) \Gamma \psi(\mathbf{y}) f(\mathbf{x} - \mathbf{y}) \bar{\psi}(0) \Gamma \psi(0) \rangle \quad (2)$$

where  $x = (\mathbf{x}, t)$  and  $y = (\mathbf{y}, t)$ , and the gauge is fixed to Landau gauge. With  $f(\mathbf{x} - \mathbf{y}) = \delta_r(|\mathbf{x} - \mathbf{y}| - r)$ , we calculate the quantity  $C(r, t) = G_{\delta_r}(t)$  shown in Fig. 7. We then use the asymptotic value  $C_0(r) \equiv C(r, \infty)$  to define an extended sink correlation function  $G_{ext}(t) \equiv G_{C_0}(t)$ . The functions  $C(r, t)$  stabilizes at approximately  $t/a = 10$ , representing the meson final state “wave function.”

Figure 7. Extended sink functions  $C(r, t)$  for various  $t/a$ .Figure 8. Vector meson spectrum for  $am_q \leq 0.1$ .

The use of extended sinks was most valuable in the calculation of the vector meson spectrum, due to the increase in the size of the fitting window. The point sink and extended sink vector meson spectra are compared in Fig. 8 for low quark mass,  $am_q \leq 0.1$ . A fit of the quark-mass dependence of the vector meson mass obtained from the extended sink data gives

$$aM = 0.4159(11) + 1.044(16)a(m_{q1} + m_{q2})/2 \quad (3)$$

### 2.3. Quenched chiral logs

The sharp rise at low  $am_q$  of the ratio of the pseudoscalar mass squared  $(aM)^2$  to  $(am_{q1} + am_{q2})$ , which we observe in Fig. 9, can be interpreted as an indication of quenched chiral logs. A value for the quenched chiral log parameter  $\delta$  was obtained via a fit to the expression  $y = 1 + \delta x$  [5],

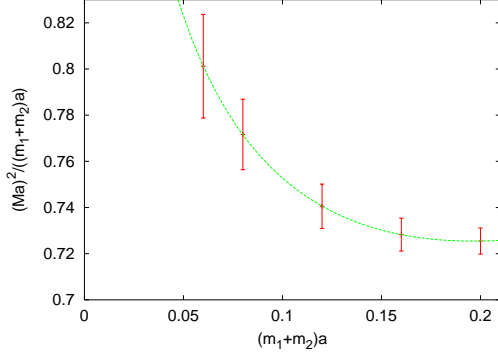


Figure 9. Evidence for quenched chiral logs.

where

$$y = \frac{2m_1}{m_1 + m_2} \frac{M_{12}^2}{M_{11}^2} \times \frac{2m_2}{m_1 + m_2} \frac{M_{12}^2}{M_{22}^2} \quad (4)$$

and

$$x = 2 + \frac{m_1 + m_2}{m_1 - m_2} \ln \left( \frac{m_2}{m_1} \right). \quad (5)$$

The resulting value for  $\delta$  in the PP-SS channel is  $\delta = 0.13 \pm 0.09$ .

We fit the degenerate quark mass PP-SS channel results to the expression

$$(Ma)^2 = A(ma)^{1/(1+\delta)} + B(ma)^2 \quad (6)$$

where  $M$  is the PP-SS mass and  $m = m_{q1} + m_{q2}$ . The fit is shown in Fig. 9, and the results for the parameters are

$$A = 0.441(1), \quad B = 0.604(3), \quad \delta = 0.243(1), \quad (7)$$

consistent with the value of  $\delta$  obtained above as well as elsewhere [5,6,7]. Note that a fit to  $(Ma)^2$  in Eq. (6) containing an additional constant term  $C$  does not change the central values of  $A$ ,  $B$ , or  $\delta$  and produces a value for  $C$  that is very small and consistent with zero.

### 3. Baryon Results

In calculating the baryon spectrum, we found that caution is needed in determining an appropriate fitting window for the correlation functions, due to fluctuations at large  $t$ .

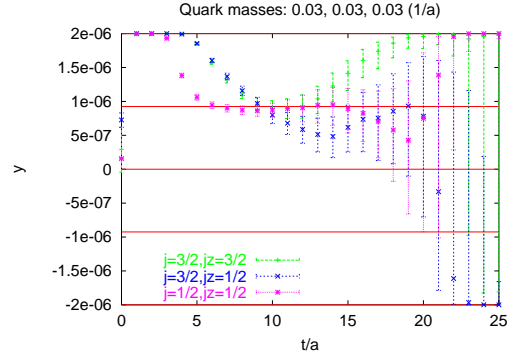


Figure 10. Caution about fluctuations.

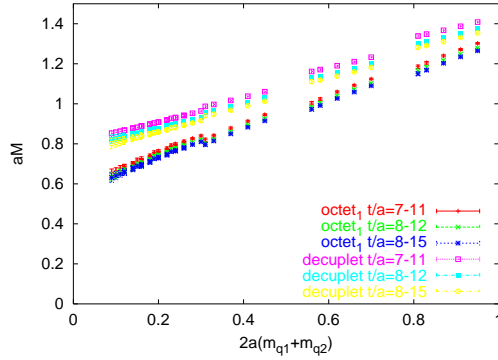


Figure 11. Baryons: octet and decuplet spectra for various fitting windows.

Shown in Fig. 10 are the average baryon propagators for the octet and decuplet, after multiplication by  $\exp(0.65t/a)$  and the mapping  $y \rightarrow 2d \tanh[y/(2d)]$ ,  $d = 10^{-6}$ . The mapping allows for a clear exposition of the fluctuations.

Fig. 11 shows the octet and decuplet baryon masses vs. total quark mass for all quark mass combinations where two of the quarks have the same mass  $m_{q1}$ , while the third quark has mass  $m_{q2}$ , and for various correlator fitting windows. The sensitivity to the fitting window is apparent. The ultimate fitting window chosen was  $8 \leq t/a \leq 15$ .

Fig. 12 shows the low quark mass spectrum, with fitting window  $8 \leq t/a \leq 15$ , for the two

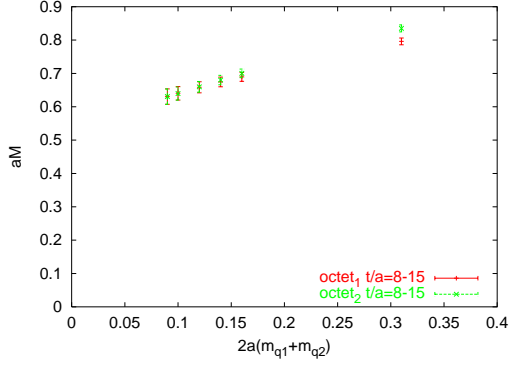


Figure 12. Spectra for the two octet baryon states discussed in the text.

octet states

$$8_1 = (|\uparrow\downarrow\uparrow\rangle - |\downarrow\uparrow\uparrow\rangle)/\sqrt{2} \quad (8)$$

$$8_2 = (|\uparrow\downarrow\uparrow\rangle + |\downarrow\uparrow\uparrow\rangle - 2|\uparrow\uparrow\downarrow\rangle)/\sqrt{6} \quad (9)$$

with  $am_{q1} = 0.03$  and  $0.03 \leq am_{q2} \leq 0.25$ . The corresponding correlation functions become identical for  $m_{q2} = m_{q1}$ , but would describe  $\Lambda$ ,  $\Sigma$ -like states, respectively, for  $m_{q1} \neq m_{q2}$ .

Fig. 13 shows the degenerate quark mass octet and decuplet spectrum for low quark mass ( $am_q \leq 0.1$ ) again with fitting window  $8 \leq t/a \leq 15$ . Extrapolating to the chiral limit we get  $aM_8 = 0.562(4)$ ,  $aM_{10} = 0.747(3)$ ,  $aM_\rho = 0.4159(11)$ , and correspondingly

$$M_\rho/M_8 = 0.740(7) \quad (10)$$

$$M_{10}/M_8 = 1.329(11) \quad (11)$$

while experimentally  $M_\rho/M_N = 0.820$  and  $M_\Delta/M_N = 1.312$ .

#### 4. Conclusion

Our results show that use of the overlap formulation is practical, albeit computationally costly, for the calculation of quark propagators on large lattices, and validate the good chiral properties of this discretization. Work in progress includes the evaluation of quark correlation functions in baryon final states and quenched calculations on a  $14^3 \times 48$  lattice at  $\beta = 5.85$  to investigate scaling.

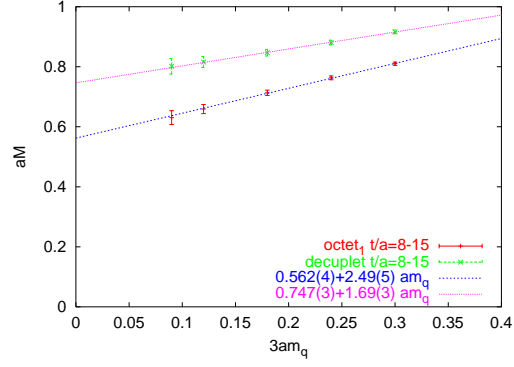


Figure 13. Baryons for  $am_{q1} = am_{q2} \leq 0.1$ .

#### REFERENCES

1. F. Berruto, N. Garron, C. Hoelbling, L. Lellouch, C. Rebbi and N. Shores, Nucl. Phys. Proc. Suppl. **129-130**, 471 (2004) [arXiv:hep-lat/0310006].
2. F. Berruto et al., presentation by L. Lellouch at this conference.
3. L. Giusti, C. Hoelbling and C. Rebbi, Phys. Rev. D **64**, 114508 (2001) [Erratum-ibid. D **65**, 079903 (2002)] [arXiv:hep-lat/0108007].
4. S. Hauswirth, arXiv:hep-lat/0204015.
5. S. Aoki *et al.* [CP-PACS Collaboration], Phys. Rev. D **67**, 034503 (2003) [arXiv:hep-lat/0206009].
6. H. Wittig, Nucl. Phys. Proc. Suppl. **119**, 59 (2003) [arXiv:hep-lat/0210025].
7. C. Gattringer *et al.* [BGR Collaboration], Nucl. Phys. B **677**, 3 (2004) [arXiv:hep-lat/0307013].